

Supernova Reverse Shocks and SiC Growth

Ethan A.-N. Deneault¹, Donald D. Clayton²

Department of Physics and Astronomy, Clemson University, Clemson, SC 29634

Alexander Heger³

Department of Astronomy and Astrophysics, University of Chicago, Chicago, IL 60637

ABSTRACT

We present new mechanisms by which the isotopic compositions of X-type grains of presolar SiC are altered by reverse shocks in Type II supernovae. We address three epochs of reverse shocks: pressure wave from the H envelope near $t = 10^6$ s; reverse shock from the presupernova wind near 10^8 - 10^9 s; reverse shock from the ISM near 10^{10} s. Using 1-D hydrodynamics we show that the first creates a dense shell of Si and C atoms near 10^6 s in which the SiC surely condenses. The second reverse shock causes precondensed grains to move rapidly forward through decelerated gas of different isotopic composition, during which implantation, sputtering and further condensation occur simultaneously. The third reverse shock causes only further ion implantation and sputtering, which may affect trace element isotopic compositions. Using a $25M_{\odot}$ supernova model we propose solutions to the following unsolved questions: where does SiC condense?; why does SiC condense in preference to graphite?; why is condensed SiC ^{28}Si -rich?; why is O richness no obstacle to SiC condensation?; how many atoms of each isotope are impacted by a grain that condenses at time t_0 at radial coordinate r_0 ? These many considerations are put forward as a road map for interpreting SiC X grains found in meteorites and their meaning for supernova physics.

Subject headings: —supernova remnants —dust extinction —infrared:stars —astrochemistry

1. Introduction

Presolar grains which were trapped in the assembly of the parent bodies of meteorites are extracted and studied in terrestrial laboratories (Bernatowicz & Zinner 1997). Dramatic isotopic anomalies (in comparison with solar isotopic abundances) identify these grains as being presolar

¹edeneau@antares.phys.clemson.edu

²cdonald@clemson.edu

³alex@oddjob.uchicago.edu

and even identify, in many cases, the type of stellar mass loss within which they condensed. The most thoroughly studied types of grains are silicon-carbide crystals (see Amari, Nittler, Zinner, Lodders, & Lewis 2001, for a recent discussion of the families of SiC particles). In particular, SiC type-X grains condensed within the interiors of supernovae during their expansion and cooling (Amari, Hoppe, Zinner, & Lewis 1992; Clayton, Amari, & Zinner 1997a). This paper will concern itself mainly with this SiC supernova condensate (SuNoCon). We first present arguments for which volume element of the supernova the SiC grains condense within, and later discuss why SiC can condense at all. We also will present arguments about why silicon found in SiC is isotopically light in comparison with solar isotopic composition; and in the same spirit why isotopically heavy Si in supernova SiC grains is rare. An SEM photograph of one such X grain (L. Nittler, private communication) can be seen in Figure 1, whose caption illustrates the dramatic isotopic anomalies in these grains.

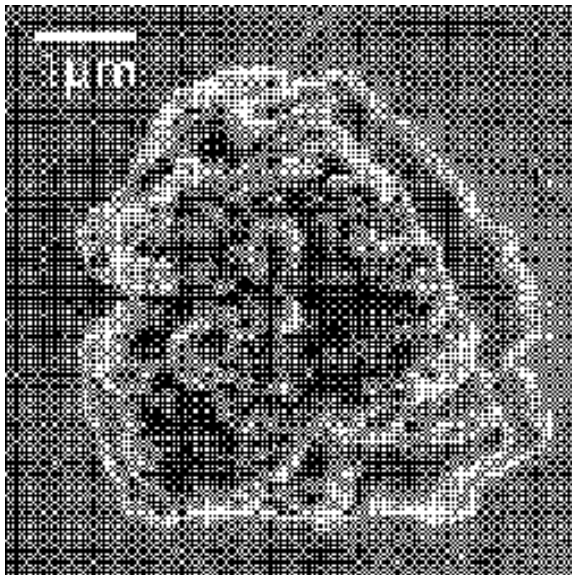


Fig. 1.— SEM photograph of SiC grain KJGM4-244-2 from the Murchison meteorite (courtesy of Larry Nittler). $^{12}\text{C}/^{13}\text{C} = 364 \pm 18$, $^{14}\text{N}/^{15}\text{N} = 82 \pm 3$ in bulk. The highly inhomogeneous appearance of this grain has never been explained, although it looks like a collection of smaller grains fused together. Such a possibility is predicted in section 6.4 whenever the large grains overtake smaller ones following a reverse shock.

A major problem in SuNoCon interpretation has been that although the grains clearly condensed within supernova interiors, it is not clear from which parcels of gas the grains condensed. Some authors (e.g., Travaglio, Gallino, Amari, Zinner, Woosley, & Lewis 1999) postulate mixing matter from different, selected portions of the supernova interior at the molecular level prior to thermal condensation; but the requisite timescale for this mixing appears to us to be too long (e.g.,

Clayton 1999; Clayton, Meyer, & The 2000) In addition, such an ad hoc theory does not explain why many other isotopic compositions that can be obtained from arbitrary mixes are not found in the laboratory inventory of SiC SuNoCons. We suggest the possibility of mixing of a different type; namely, grain motion forward at high speed following the slowing of the gas by reverse shocks. This new proposal was recently advanced by Clayton, Meyer, The, & El Eid (2002). We point to importance of three distinct reverse shocks in Type II supernovae and suggest their possible cosmochemical importance for the origin of the observed SiC grains. We study this question anew within the framework of the new 1-D supernova calculations by Rauscher, Heger, Hoffman, & Woosley (2002), focusing on their $25M_{\odot}$ model s25, which was exploded with a final kinetic energy of 1.2×10^{51} ergs. These models are further described by Woosley, Heger, & Weaver (2002), hereafter WHW.

2. Reverse Shocks

At least three reverse shocks are significant for the condensation of SiC. Our goal is to discuss the implications of these shocks for the observed SiC X grains from supernovae. Our scientific results are new ideas and their possible implications rather than a study of the shocks themselves, for which many uncertainties and complications exist. We will idealize the shocks as seems befitting for an initial discussion of their chemical consequences.

2.1. Reverse shock rebounded from the core/envelope interface

This reverse shock is reflected in 1-D hydro from the large density decrease in the H envelope above the He core. In 10^6 s it has propagated back inward (in mass coordinate) to $m = 3$ where it establishes a large peak in the density between $m = 2.7$ and $m = 3.6$. Figure 2 plots the product $t^3 \rho(t)$ versus radial mass coordinate because that structural product is unchanging during epochs of homologous expansion; therefore, it reveals nonhomologous expansion as time-dependant structural changes. Figure 2 compares the density structure at several values of the time to show what can be seen more dynamically in an animation. This animation, showing density, velocity and temperature versus mass coordinate is Figure 3 In Figure 3, the viewer will note that this density peak has not yet been established at $t = 10^5$ s. It is a nonhomologous structure set up by the interaction of pressure waves, even if the supernova occurs within a vacuum. There it can be seen that momentum flux toward that shell compresses it to higher pressure and density than the surrounding material. The cause of the inward (in mass) pressure wave that establishes this density peak is the increase radially of the product ρr^3 in the presupernova structure in the hydrogen envelope (see Figure 9 of Herant & Woosley (1994) or WHW, Figure 25). Increasing ρr^3 causes deceleration of the outward shock, causing the pileup of hot shocked matter that sends the pressure wave inward in mass coordinate. In space, the trailing material runs into the higher pressure region caused by the deceleration of the forward shock.

The mass interval $2.7 < m < 3.6$ moves outward as a shell of fixed thickness (approximately)

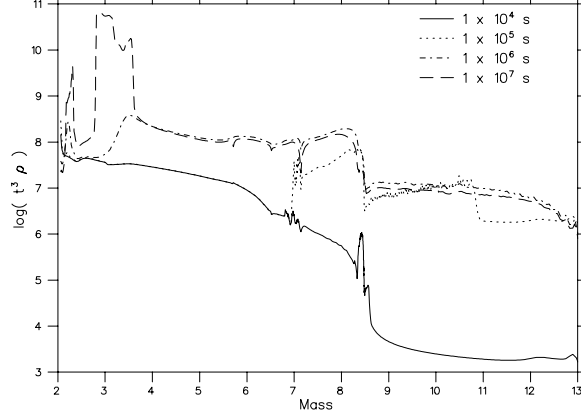


Fig. 2.— The density structure $t^3 \rho$ versus m at several values of post-explosion time. Note the large density enhancement in the region $2.7 < m < 3.6$. The huge increase at $m > 8$ for $t < 10^5$ s represents the increase of the factor t^3 prior to the arrival of the shock.

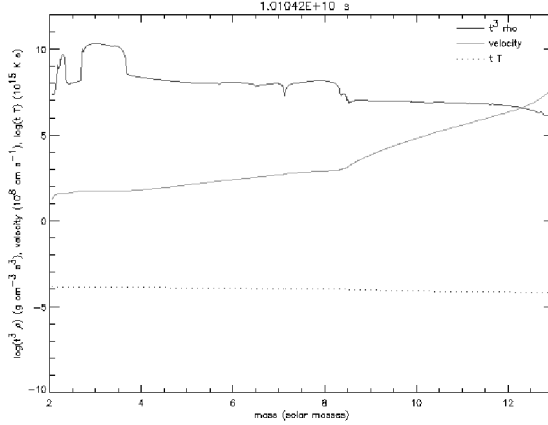


Fig. 3.— An animation which plots density, temperature, and velocity as a function of mass coordinate. This animation more explicitly reveals the growth of the large density enhancement found in Figure 2.

from 10^6 to 10^8 seconds, confined by the momentum flux into it, after which it expands homologously from 10^8 to 10^{10} seconds. The more dense subshell $2.85 < m < 3.15$ has more extreme hydrodynamic behavior. Its thickness actually decreases dramatically between 10^6 to 10^8 seconds, its density squeezed upward by the momentum flux into it, after which it expands homologously from 10^8 to 10^{10} seconds. Figure 4 shows the radial thickness of both mass intervals at selected decades of time. For the mass interval $2.7 < m < 3.6$, the near constancy until $t = 10^8$ s is replaced by a linear expansion for larger t . For the more dense subshell $2.85 < m < 3.15$ the width first decreases sharply before resuming its participation in a new homologous expansion. The factor of

100 decrease of the width before 10^7 s is consistent with the constancy of the mass contained in a shell whose density remains constant while the scale of the supernova remnant increases by the factor 10^2 . This very dramatic behavior indicates this mass interval as a probable one for dust condensation.

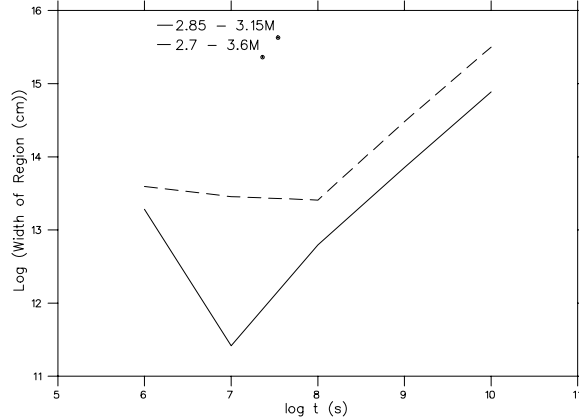


Fig. 4.— The radial width of two mass intervals is shown for selected values of time. The width of the more dense subshell $2.85 < m < 3.15$ declines by a factor 10^2 before 10^7 s because its density is held almost constant over that interval by momentum flux. The larger shell $2.7 < m < 3.6$ reveals less extreme compression by the momentum flux that has singled out this region in our 1-D calculation.

The large density bump will dominate the SiC condensation structure functions to be described in section 3. Not only is this shell more dense than other supernova matter but its density declines with time more slowly than t^{-3} during the crucial period for grain growth prior to 10^8 s. It may be questioned whether the 1-D hydro code that prepared this data is adequate for the SiC condensation. Herant & Woosley (1994) showed with 2-D Smooth Particle Hydrodynamics (SPH), that significant velocity mixing occurs even without an externally launched reverse shock (See also Kifonidis, Plewa, Janka, & Müller 2000). The thin shell in Figure 2 will surely not be stable in the face of reverse shocks, and the question then arises whether the density enhancement is an artifact of 1-D simulation. For a convincing answer, we must await 3-D simulations of the reverse shocks within young supernova ejecta; however the following can be speculated. Although the thin mass shell may in fact break up into “clouds”, those may be dense in comparison with the surroundings for the same reasons that the 1-D shell is dense, and if so, the dominance of SiC condensation within this matter may remain. For the time being we emphasize, with this limitation, the wholly remarkable fact of a dense shell of SiC being established exactly at the epoch of grain condensation by purely hydrodynamical interactions. This appears to be an unforeseen event, relevant to physical models of SiC condensation.

Within this context it is important to ask about molecular mixing within the density peak. Is

diffusion sufficiently fast to mix it to a degree that the natural association of $^{29,30}\text{Si}$ with ^{28}Si is explained by condensation from a mixed gas. We repeat Clayton (1999)’s argument in this specific context to highlight his negative conclusion. The width of the high density peak at 10^7s is about $\Delta r = 10^{12}\text{cm}$, so the argument consists of showing that diffusion lengths during a year are very much less than 10^{12}cm . With a number density $n = 10^{12}\text{cm}^{-3}$ the mean free path $d = 10^4\text{cm}$ if the scattering cross section is taken to be 10^{-16}cm^2 . With a temperature of 2000K while condensation is beginning, the thermal speed is $v_T = 1.6 \times 10^5\text{cm s}^{-1}$ if the mean weight $A = 20$. Thus an atom scatters 16 times per second. If its scattered direction is taken to be isotropic, the mean distance diffused after N scatters is estimated by the isotropic random walk:

$$\langle x^2 \rangle^{1/2} = D = d \left(\frac{N}{3} \right)^{1/2} \quad (1)$$

Within a year the number of scatters N at the rate 16 s^{-1} is $N = 5 \times 10^8$, giving the mean distance $D = 2.2 \times 10^8\text{cm}$. This distance is much less than the shell thickness $\Delta r = 10^{12}\text{cm}$, showing that molecular diffusion mixes the matter a negligible amount. Even if 3-D calculations confirm, as they surely will, that this thin shell breaks up, the turbulent “clouds” that can be established during a year will still have sizes greater than 10^8cm , so that diffusion is still ineffective except over these 10^8cm interfaces between much larger turbulent cells. Based on this argument, we hereafter assume that some other physical mechanism is responsible for causing ^{28}Si -rich SiC initial condensates to obtain about half their solar complement of heavy Si isotopes. We suggest, following Clayton et al. (2002), that subsequent reverse shocks must accomplish this.

2.2. Reverse shock from massive stellar winds

Because of mass loss in the red-supergiant phase, stars initially more massive than $20M_\odot$ have a large circumstellar shell of perhaps 1-20 solar masses, depending on the initial mass and on the mass-loss rates. The new WHW model for a $25M_\odot$ supernova loses $12M_\odot$ of material, leaving $13M_\odot$ remaining at the time of explosion. The $12M_\odot$ of circumstellar material generates a strong reverse shock that propagates back, in mass coordinate, into the nucleosynthesis ejecta on a timescale of months to years, depending on the structure of the circumstellar material. Spatially, the ejecta runs into the high pressure created by the shock from the wind.

When this reverse shock arrives in the SiC growth region (at a time between 6 months, when SiC growth begins, and three years, when SiC growth is very nearly complete) a new mixing mechanism is created for SiC growth. The condensing grains move forward through the decelerated gas while SiC condensation is still occurring, sampling a large range of nuclear compositions. This, in effect, mixes the composition for the condensing grain. This consideration moves condensation science into previously unstudied conditions. Namely, the reverse shock heats the gas to temperatures that are too high for condensation in any equilibrium sense; but the precondensed grains from the previously cold flow remain much cooler than the gas. If a grain moves forward at 500 km s^{-1} through the decelerated gas, as we show below, the power input to a $1\text{ }\mu\text{m}$ grain owing to collisions

with atoms at $N = 10^{12}\text{cm}^{-3}$ is about 10 erg s^{-1} . That power can be radiated by infrared emission at $T_g = 1100\text{ K}$. Gas temperatures of 10^6 K also can not heat the grains much above 1000 K . Thus the condensed grains will not evaporate. Indeed, they may even continue condensation within the hot shocked gas!

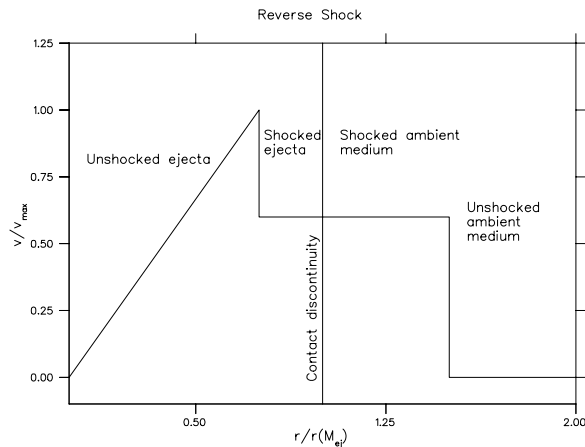


Fig. 5.— *Schematic of the velocity profile of the ejecta after a reverse shock has reentered the ejecta. The velocity increases linearly with distance (homologous expansion) up to a maximum V_{max} at the radius reached by the reverse shock. Note that the radial distance is measured by a mass coordinate labeling that radius, where unity is the contact surface between ejecta and circumstellar material.*

Figure 5 is a schematic depiction of the velocity profile established by reverse shocks (see also Truelove & McKee 1999). Velocity increases linearly with radial distance within the ejecta that has not yet been shocked by collision with the wind to a maximum V_{max} at the location of the reverse shock. External to that shock, the already shocked ejecta has assumed a nearly constant velocity within the remainder of the ejecta. That velocity is about 60 % of V_{max} , and as the shock propagates inward (in mass coordinate, not in space), the value of V_{max} declines according to Figure 5 and the external velocity correspondingly declines to maintain a constant velocity near 60 % of V_{max} . Despite this being an approximation, we assume it to enable discussion of the cosmochemical consequences. Notice that the already shocked ejecta is moving outward as a shell (uniform velocity) whereas the unshocked ejecta expands homologously until the shock reaches it.

Figure 6 illustrates the situation for a thermally condensed grain within the ejecta as the shock reaches it. Hydrodynamic forces slow the gas to about $0.60 V_{max}$, but the grain can not be slowed so rapidly; hence it moves forward with a relative speed $\Delta V = 0.40 V_{max}$. If the dense shell $2.7 < m < 3.6$ moves near 1500 km s^{-1} , for example, the grain will move forward through the hot shocked gas at speed $\Delta V = 600\text{ km s}^{-1}$. At such speeds atoms striking the grain will be implanted to depths near 0.05 micron within the grain, and will also cause sputtering from the grain surface. The grain temperature, however, will remain near 1000 K , so evaporation will not occur. Only sputtering can remove atoms at this time. This relative speed is about 50 % greater

than the familiar speed of the solar wind, kinetic energy near 1-2 keV per nucleon. A large literature studied the sputtering and implantation of solar wind into lunar fine soil during the Apollo program (Zinner, Dust, Chaumont, & Dran 1978; Kiko, Kirsten, & Ries 1978). Because the sputtering yield is near unity, the grain will only slowly gain or lose mass; but the identity of the atoms within it may evolve. This conclusion has already been presented Clayton et al. (2002). Although the photonic emission from these shocks has been well studied (Chevalier & Fransson 1994; Fransson, Chevalier, Filippenko, Leibundgut, Barth, Fesen, Kirshner, Leonard, Li, Lundqvist, Sollerman, & Van Dyk 2002), their chemical implications for thermal condensates has not.

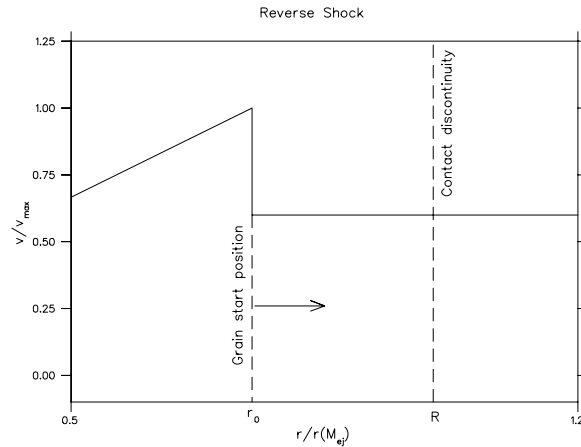


Fig. 6.— *Schematic of the relative velocity forward of already condensed grains after the reverse shock has slowed the flow to about $0.6V_{max}$ (see Figure 5). The grains move forward with relative velocity $0.4 V_{max}$ into the already shocked ejecta.*

2.3. Reverse shock from interstellar medium

A huge literature exists (Truelove & McKee 1999) for this interaction, both for the X ray emission from the shocked ambient medium and for the emission from the reheated ejecta by the reverse shock. If the ISM is as dense as compact HII regions, this reverse shock will reenter the ejecta, and will decelerate the gas with respect to the high-inertia SiC grains, which will have already condensed. This will cause sputtering and ion implantation as the grains then propagate outward through the slowed gas, as was originally envisioned by Clayton et al. (2002) within this context of a reverse shock from the ISM. At these late times, the grains may have actually emerged from the supernova interior. They will be warm enough for IR radiation but their interactions will consist entirely of sputtering and ion implantation, which occurs throughout their outward journey through the overlying column of atoms.

3. The SiC condensation-structure functions

The condensation of SiC is not as well understood kinematically as is the condensation of graphite. For graphite, it was possible to construct (Clayton, Liu, & Dalgarno 1999; Clayton, Deneault, & Meyer 2001) an explicit kinematic model: stationary molecular abundances of linear chains C_n ; isomerization of linear C_n into ringed C_n , which is more resitive to oxidation; rapid attachments of C atoms to rings, which graphitize during the process. The condensation of SiC will occur in gas that is not only heavily oxidizing, but in which the relative abundances of Si and C vary rapidly with location. Using the mass fractions of Si and of C as function of radial mass in $25M_\odot$ model by Rauscher et al. (2002), the SiC structure functions to be defined below indicate that Si will be more abundant than C in the dense shell that is established near $m = 3$, and that SiC will condense there.

Without a full theory of dynamic SiC condensation, we can nonetheless motivate where in the supernova that it should occur most prolifically. We do this with densities of the reacting species Si and C near 10^7 s, as in Figure 2.

3.1. SiC molecule-formation-rate structure function

Figure 7 shows the product $n(C)n(Si) \text{ cm}^{-6}$ which provides the source term for SiC molecules. One expects SiC solids to grow in regions where SiC molecules are rapidly made. This figure shows a huge bump between $m = 2.7$ and $m = 3.6$. As described below, silicon is light (^{28}Si -rich) in the inner half and heavy ($^{29,30}\text{Si}$ -rich) in the outer half. The number density of Si atoms in this density peak at $t = 10^7$ s is $n(\text{Si})=10^{11}\text{cm}^{-3}$, several magnitudes greater than in surrounding material. We therefore take it that SiC X grains must condense here.

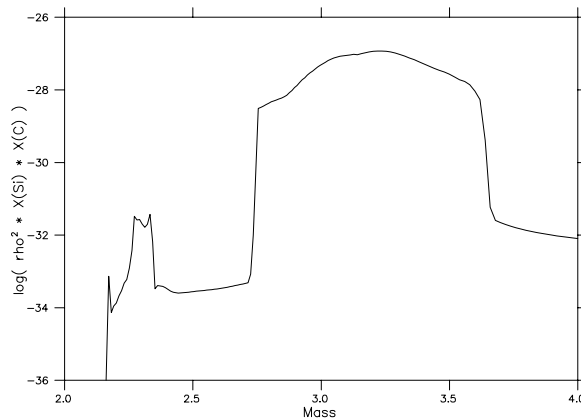


Fig. 7.— *First SiC structure function. The product $n(C)n(Si) \text{ cm}^{-6}$ which provides the source term for SiC molecules. One expects SiC solids to grow in regions where SiC molecules are rapidly made.*

We follow Clayton et al. (1999, 2001) in assuming that the buildup of CO and SiO molecules is counteracted by radiative disruption, enabling SiC solids to condense even in regions where $O > C$. The reader must not be disturbed at the thought of disruption of SiC by the same process, because SiC can react rapidly by chemical means whereas CO can not. This is a fundamental distinction. Small SiC crystals are destroyed (in part) by their chemical growth to larger SiC structures. Thus CO and SiO destruction restores free C and Si to the gas (See Clayton et al. (2001) for a detailed pathway in the case of graphite condensation). Our supposition that SiC solids condense quite well in O-rich radioactive gas rests on the idea that when a condensation nucleus already exists (SiC), it condenses further Si and C from the free atoms in the gas faster than the free O atoms can destroy SiC solids. To be sure, O collisions with the grain are more frequent, but the oxidation of SiC solid is slower because of the additional need for the O atoms to break the SiC bonds to remove an integrated atom from a small crystal. The Si and C atoms, on the other hand, can simply bond and stick. Clayton et al. (2001) discussed this transition to slower oxidation rates for the graphite case, and we shall assume that the SiC case is similar. Condensation in an oxydizing gas was not believed to be possible by Travaglio et al. (1999), who hypothesized that ^{28}Si -rich inner-core silicon could mix at the molecular level with enough C-rich gas from the He shell to condense SiC in C-rich mixtures.

A smaller peak can be found between $m = 2.2$ and $2.4 M_{\odot}$, in a region of pure ^{28}Si , but as will be shown in the next section, its contribution to the formation of SiC grains is negligible.

3.2. SiC maximal-growth structure function

Figure 8 shows a second SiC structure function. It presumes that condensation of SiC is so efficient that it completely depletes the element of lesser abundance. In other words, condensation of SiC depletes all Si wherever C is more abundant and all C wherever Si is more abundant. Figure 8, in that sense is a graph of the maximum mass density of SiC. It is the product of the supernova density ρ with the mass fraction of the lesser of the two elemental mass fractions, augmented by the factor $40/A_{\text{lesser}}$, where $A_{\text{lesser}} = 12$ if C is less abundant and 28 if Si is less abundant. This product represents the maximum density of SiC that could possibly condense at each mass coordinate:

$$\rho(\text{SiC}) = \rho X_{\text{lesser}}(C, O) \frac{40}{A_{\text{lesser}}} \quad (2)$$

This shows that the mass zone of enhanced density, $2.7 < m < 3.6$, also has the greatest capacity to condense SiC mass when the less abundant species is totally depleted in SiC formation. The smaller peak, found between 2.2 and $2.4 M_{\odot}$ in Figure 7 has no such capacity for grain formation, even though the rate in that region is comparable. The integrated number of collisions is adequate to deplete condensibles if nucleation sites are able to form early. Clayton et al. (1999) were able to give such a kinetic theory of nucleation for graphite, but such a compelling picture does not yet exist for SiC. Without adequate population control (Clayton et al. 2001) these nucleation sites can

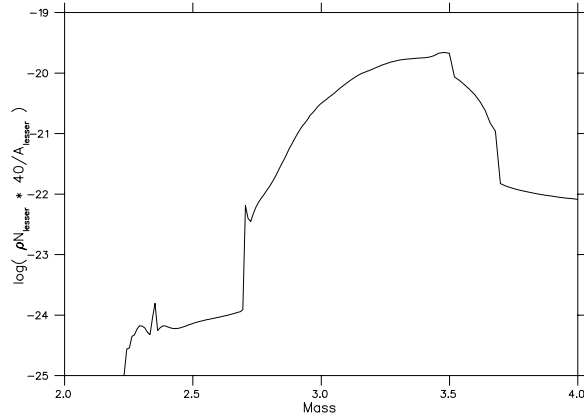


Fig. 8.— *The maximum mass density of SiC given by the concentration of the lesser of the two constituents.*

be too abundant, in which case the depletion is total but results in large numbers of tiny particles rather than the micron-sized examples found abundantly in the meteorites.

Faced with these uncertainties we will in what follows assume that the depletion of lesser abundance is total but that its numbers are sufficiently restricted to allow each grain to grow large. That is what the experimental data for micron-sized SiC demonstrates.

4. Why do supernovae condense SiC at all?

Supernova SiC X grains are rather common, comprising about one percent of the number of SiC grains condensed in C-star winds. Several authors (Bernatowicz et al. 1996; Sharp & Wasserburg 1995) have shown that in C stars graphite will condense prior to SiC unless the C/O ratio is no more than just slightly greater than unity. (See Figure 10 of Bernatowicz et al.). This restriction on the C/O ratio derives, however, from the assumption that CO formation will lock up available carbon, in which case, if C/O only slightly exceeds unity, the free C is no more abundant than is Si, with the result that SiC can condense.

But in supernovae, the CO molecule can not permanently bind up the C atoms. Given solar abundances, graphite will then condense prior to SiC and deplete the C. If graphite condenses first, the question arises “Why, then, do supernovae condense SiC?”. This simple question appears not to have been clearly answered in the literature; therefore we shall address it here. SiC condenses in preference to graphite when the free Si abundance exceeds by a factor ten or more the free carbon abundance. In such circumstances, not only does the equilibrium favor SiC condensation, but any graphite nuclei that do grow will be rapidly converted to SiC by the much more numerous Si atoms. It is important in this regard to remember that the grains will be cooler than the gas, even during the condensation epoch, owing to their infrared cooling.

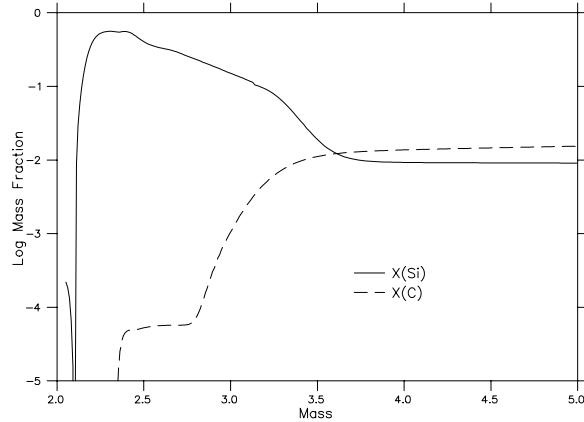


Fig. 9.— *Mass fractions of Si and C in the $25M_{\odot}$ supernova (WHW). Graphite is expected to condense first, depleting C whenever they are comparably abundant. To condense SiC requires $\text{Si} > \text{C}$. Accordingly we focus on the region inside $m = 3.2$, where $\text{Si}/\text{C} > 10$, as the supernova portion wherein SiC is a major condensate.*

Figure 9 shows the mass fractions of Si and C in the $25M_{\odot}$ supernova (Rauscher et al. 2002). Interior to $m = 3.4$ the abundance of Si exceeds that of C; and within $m = 3.2$ by an order of magnitude and more. This region lies squarely within the density peak ($2.7 < m < 3.6$) shown in Figure 1

It would be misleading to simply apply equilibrium condensation theory to this situation because the condensation has kinetic controls that cause the condensates to differ slightly from equilibrium; and presenting condensation theory (e.g., Sharp & Wasserburg 1995) is not our purpose. Our present goal is met by the simple assumption that SiC condenses wherever Si is at least tenfold more abundant than C. Figure 9 then targets the zone $2.7 < m < 3.2$. If a Si/C ratio of 100 is instead required, this same argument targets the zone $2.7 < m < 3.0$ instead. Accordingly, we postulate that SiC SuNoCons form in this matter only. At larger m , graphite depletes the carbon before SiC condensation can occur.

5. Why are supernova SiC grains ^{28}Si -rich?

The ^{28}Si excess within SiC X grains is one of the defining characteristics of supernova SiC. But why? It is surely not adequate to simply say that “Supernovae make a lot of ^{28}Si -rich Si”, because, as Figure 10 shows, they also make a lot of ^{29}Si and ^{30}Si -rich silicon. Where, then, are the $^{29,30}\text{Si}$ -rich SiC X grains? We now believe that an answer to this question also can be given.

Based on the results of section 4, we anticipate that SiC condenses (in the $25M_{\odot}$ supernova) within the zone $2.7 < m < 3.0$ - 3.2 . When the integrals over the mass in that region are performed,

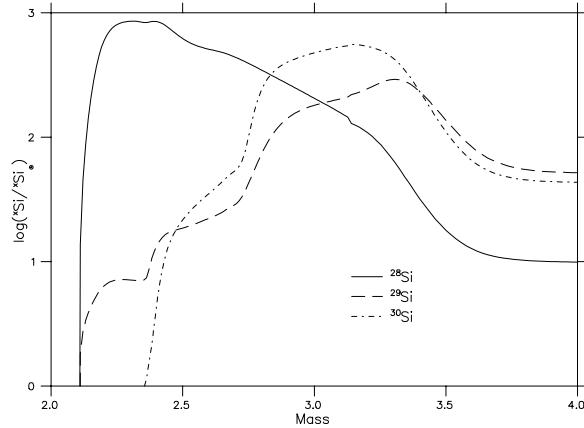


Fig. 10.— *Overabundances of the Si isotopes in the $25M_{\odot}$ supernova with solar initial abundances. The ^{28}Si -rich portions are inside $m = 2.8$. If presolar supernovae had $Z = 0.5$ solar rather than solar, the ^{28}Si -rich zone would extend to about $m = 3.0$. Bulk Si/C is much greater than unity within $m = 3.0$.*

the data leading to Figure 10 confirm that the $^{29}\text{Si}/^{28}\text{Si}$ ratio is between 1/3 to 1/2 solar and the $^{30}\text{Si}/^{28}\text{Si}$ ratio is slightly in excess of solar for stars having initial solar abundances. However, the presolar supernovae responsible for the X grains exploded more than 5 Gyr ago. Considering also the excess metal richness of the sun for its location in the galaxy we can conclude that the average presolar supernova would have been perhaps half solar in its initial metallicity. In this case the entire Si-rich zone is also ^{28}Si -rich in its Si. The caption of Figure 1 describes the isotopic signature of that grain, which is typical for this class of SiC X grains. It is for this reason that SiC X grains are ^{28}Si -rich. The matter outside $m = 3.0 - 3.2M_{\odot}$ condenses graphite rather than SiC, as shown in section 4, therefore we see why the $^{29,30}\text{Si}$ -rich SiC X grains do not exist.

This is demonstrated in Figure 11 for a presolar supernova of half solar metallicity. That is, the supernova $^{29}\text{Si}/^{28}\text{Si}$ and $^{30}\text{Si}/^{28}\text{Si}$ ratios are, in each mass shell m , taken to be half of the values calculated in the solar-metallicity $25M_{\odot}$ model by WHW. Timmes & Clayton (1996) demonstrated that such a procedure obtains reliable results. The formatting of the plotted points, shell by shell, uses triangles inside $m = 3.2$ and circles outside. They make it evident that the normalized ratios are largely less than unity within $m = 3.2$ and become greater than unity outside. If the entire high-density zone $2.7 < m < 3.6$ is summed (as if it were mixed), the half-solar metallicity model gives a bulk Si characterized by $^{29}\text{Si}/^{28}\text{Si} = 0.46$ solar and $^{30}\text{Si}/^{28}\text{Si} = 0.95$ solar. With the restriction that only the zone $2.7 < m < 3.2$ is able to condense SiC, the averages for the half-solar model become $^{29}\text{Si}/^{28}\text{Si} = 0.26$ solar and $^{30}\text{Si}/^{28}\text{Si} = 0.76$ solar. Table 1 tabulates these mass ratios for three mass zones: $2.7M_{\odot} - 3.0M_{\odot}$, $3.2M_{\odot}$, and $3.6M_{\odot}$, respectively. They are even more ^{29}Si and ^{30}Si -deficient should SiC be able to condense only if the Si/C ratio is greater than 100, as discussed above.

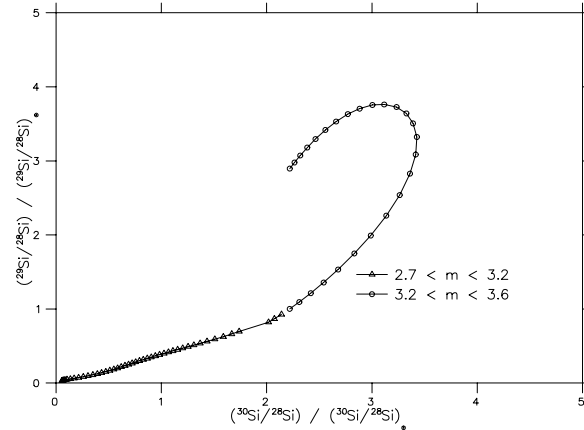


Fig. 11.— *Three-isotope plot for Si isotopes in the condensation zone. The calculated ratios for a supernova of half-solar initial metallicity are normalized to the solar value, which is what the laboratory X grains are compared with. The sequence of triangles traces the Si isotopic composition from $m = 2.7$ to $m = 3.2$; and the circles trace it through the remainder ($3.2 < m < 3.6$) of the density peak of Figure 2.*

The arguments presented here and in section 4 have shown why SiC condenses in preference to graphite in certain portions of the supernova and why that portion is isotopically light. These are the characteristics of the SiC X grains analyzed isotopically by secondary-ion mass spectrometry. We submit these ideas as a tentative road map for understanding these incredible portions of various presolar supernovae. In the next section, we return to other consequences of the reverse shocks.

6. Column Densities of Overlying Atoms

Suppose a SiC grain condenses at radial mass coordinate m (which is comoving with the SN structure). When a reverse shock arrives at m , the gas ejecta will be slowed, and the grain moves through the overlying ejecta (Clayton et al. 2002). The grains have higher inertia than the gas ejecta, and so we shall assume that their velocity remains unaffected, therefore, their relative speed will equal the amount by which the gas has been decelerated. Clayton et al. estimated that drift speed to be near 500km/s for reverse shocks in the Si-rich zones that do not arrive until 300 yr, as perhaps in Cas A; but that speed may be comparable if the ejecta encounter a massive circumstellar wind much earlier, say near 1 yr.

Clayton et al. (2002) argued that the grain will encounter the entire overlying column of atoms within the ejecta and that they will be implanted within the grains. If so, the number of atoms implanted in the grains is a function of the time when the reverse shock reaches the condensation region of the grain. Because the grain cannot slow until it has encountered a gas mass comparable to its own mass, it leaves the ejecta at almost that same relative speed if the reverse shock is at 300 yr, but it will decelerate while still within the ejecta if the reverse shock arrives within a few

years. To see this, we compute the column densities to which drifting grains will be exposed. We deemphasize the calculation of shock physics here and of the slowing of the grains in order to first emphasize the possible isotopic consequences of ion implantation.

6.1. Column density upper limit

All of our calculations were done using model s25 of Rauscher et al. (2002). Using this model, we can integrate the column densities of all isotopes, starting from the grain’s condensation radius r_0 through the overlying ejecta. SiC grains are observed to have radii of approximately one micron, so we assume that the cross sectional area of the column is $\sigma = 1 \mu\text{m}^2$. Then it is possible to compute the number of atoms that the grain will interact with by constructing a tube of constant cross section which passes through all the ejecta overlying the zone in which the grain formed.

For species AZ with mass fraction X , the total number of atoms in the column is given by:

$$N(^AZ) = \sigma \int_{r_0}^R X(r) \rho(r) \frac{N_A}{\mu_{AZ}} dr \quad (3)$$

Where R is any radius larger than r_0 , but less than or equal to that of the contact discontinuity, N_A is Avogadro’s number, and μ_{AZ} is the atomic weight of the species.

Another useful form of the integral depends on the Lagrangian mass coordinate, m . Since $dm = 4\pi r^2 \rho(r) dr$, and therefore, we can rewrite the integral:

$$N(^AZ) = \frac{N_A \sigma}{\mu_Z} \int_{m_0}^M \frac{X(m) dm}{4\pi r^2(m)} \quad (4)$$

Where m_0 and M are the grain’s starting mass coordinate and the mass coordinate of the total ejecta, respectively.

It is important to note that both of these integrals are have taken over a static structure. That is, they count all of the the atoms in the column at the time that the reverse shock arrives at the coordinate at which the grain condenses, and starts to move through the ejecta, and does not take into account the time dependent expansion of the ejecta. The entries in Table 2 can therefore be thought of as upper limits to the number of possible interactions of the grain with selected long lived isotopes of Si, Fe and Mo. Table 2 is calculated for a shock time of 10^9s , and R is the radius corresponding to the contact discontinuity. The numbers in the static column density depend on the shock time t_0 as $(10^9\text{s}/t_0)^2$.

6.2. Column density in a shell

As was described earlier in section 2.2, the circumstellar reverse shock sets up a shell structure in the ejecta. We can use this feature of the ejecta to track the grain’s motion through a constant-width region of decreasing density owing to the continued expansion of the ejecta. We define r_0 to

be the radial position where the grain condenses, and R to be the outer radius of the shell. For the purposes of our calculation below, we assume as before, that R is the radius corresponding to the interface between the He shell and the H envelope, though R can again be any radius up to that of the contact discontinuity. We construct a shell of width $R - r_0 = \text{constant}$ which is moving with the ejecta with velocity $V = 0.6V_{max}$ (see Figure 6). We have assumed, as before, the velocity of the grain to be mostly unaffected by decrease in velocity of the gas due to the reverse shock, so the grain moves through the shell at $\Delta V = 0.4V_{max} = 500 \text{ km s}^{-1}$. Since the shell's width is constant in r , the density in this shell decreases as t^{-2} .

One may ask whether it is physical to assume that the shell velocity will remain uniform over time. Looking at Figure 6 we see that the reverse shock sets up the entire shell to have the same velocity. If we consider a small Δt , V_{max} will decrease, as will the velocity of the shell, however, the shell will retain a uniform velocity. Therefore, we can consider $R - r_0 = \text{constant}$ at all times in the shell.

At some radius r' ($r_0 < r' < R$) at some time t' , the density can be written:

$$\begin{aligned} \rho(r', t') &= \left(\frac{t_0}{t}\right)^2 \rho(r', t_0) \\ &= \left(\frac{t_0}{t_0 + \Delta t}\right)^2 \rho(r', t_0) \end{aligned} \quad (5)$$

Since $\Delta t = (r' - r_0) \Delta V^{-1}$, we can re-write the time dependant term as:

$$\left(\frac{t_0}{t_0 + \Delta t}\right)^2 = \left(\frac{t_0 \Delta V}{t_0 \Delta V + (r' - r_0)}\right)^2 \quad (6)$$

We define $t_0 \Delta V = D$, where D becomes a distance parameter. Now, we can write an integral over dr' similar to equation 3:

$$\begin{aligned} N'(^AZ) &= \sigma \int_{r_0}^R X(r) \rho(r) \frac{N_A}{\mu_Z} \left(\frac{D}{D + (r' - r_0)}\right)^2 dr' \\ &= \sigma \int_{r_0}^R n(X) \left(\frac{D}{D + (r' - r_0)}\right)^2 dr' \end{aligned} \quad (7)$$

The distance parameter, D , mitigates the number of atoms that the grain can interact with. If we assume a constant velocity of the grain through the shell, then a one order of magnitude change in D changes the abundance of each atomic species by a factor 100, as shown in Figure 12. This was not unexpected, as the density of the shell decreases as t^{-2} . Figure 13 shows the dependence of the results on the initial position of the grain, r_0 . This figure shows a very important effect of the variable density of the shell. Since, as the grain moves forward into its overlying column, the density of the column is decreasing, the region that is closest to where the grain condenses has a greater effect on the grain's composition than regions farther away. As can be seen in Figure 13, grains that form between $3.2 - 3.6 M_\odot$ interact with more ^{29}Si than ^{30}Si . If grains are aggregations of smaller grains (section 6.4), the occurrence of high $^{29}\text{Si}/^{30}\text{Si}$ ratios in many X grains may be

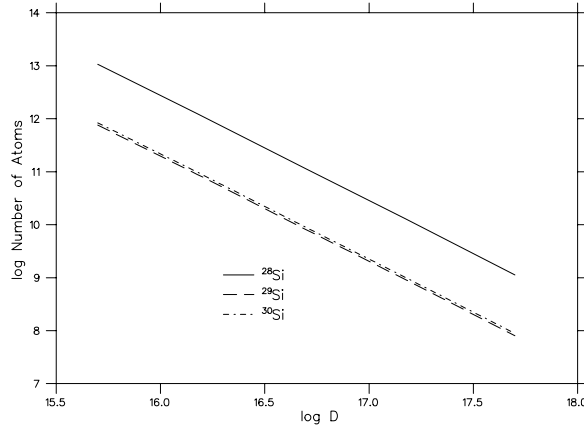


Fig. 12.— Number of Si atoms that a grain can encounter, starting from $m(r_0) = 2.6M_\odot$ as a function of the distance parameter $D = t_0\Delta V$. As ΔV is a constant, the number of atoms decreases as t_0^{-2}

explained.

Figure 13 is calculated at the specific shock time $t_0 = 3 \times 10^9 \text{ s}$. At that late time, the total number of Si atoms impacted is near 10^{10} , much less than the 10^{12} Si atoms in a $1 \mu\text{m}^2$ grain of SiC. Likewise, the number of heavier Si isotopes that could be implanted is insufficient to alter the larger numbers actually found in SiC X grains. We would thus conclude that for a shock at 100 yr the Si isotopes in SiC X grains cannot be significantly altered. For trace elements, however, such as Fe or Mo, the implantation may still dominate (Clayton et al. 2002). On the other hand, Figure 12 shows that the numbers in the $1 \mu\text{m}^2$ column decrease with shock time as $(3 \times 10^9 \text{ s}/t_0)^2$, so that a reverse shock encountered much earlier may present the SiC condensate with more Si isotopes than actually exist in the grain. A reverse shock at $t_0 = 10 \text{ yr}$, as might occur from the reaction to the presupernova wind, provides so many Si encounters that the grain encounters its own mass well before leaving the Si-rich region. This provides the new form of mixing discussed in section 2.2

Table 3 shows the total number of possible interactions between selected gas atoms and a $1 \mu\text{m}$ grain as the grain travels through the uniform-velocity shell. These numbers are bounded by the upper limits detailed in Table 2. For a grain condensing at $2.7M_\odot$, the number of possible Si implantations is very close to the upper limit of Table 2 (^{29}Si only 17% less), while the isotopes found farther out in the ejecta have significantly less than their respective upper limits, shown in Table 2. Because the density of the shell decreases as t^{-2} , regions far from the condensation of the grain have little effect, while the region that the grain condenses in has a much more pronounced effect. This influence by nearby regions is seen in Table 3. For example, the number of possible ^{100}Mo implantations increases if the grain condenses at $2.9M_\odot$ compared with $2.7M_\odot$, owing to the higher concentration of ^{100}Mo in that region. It is not practical to illustrate all of these ideas in

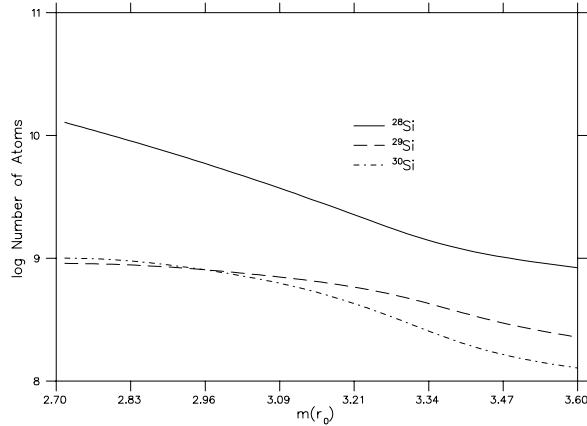


Fig. 13.— *Number of Si atoms that a grain can encounter as a function of the starting position of the grain in mass coordinate, calculated for a reverse shock at $t_0 = 3 \times 10^9$ s.*

this paper. The full versions of Tables 2 and 3 are found as electronic appendices.

6.3. Ion Implantation

The physical environment of the grains following the passage of the reverse shocks may be unique in that the grain is impacted by heavy ions of anomalous isotopic composition at kinetic energies of 1 - 2 keV per nucleon. The rate of collisions is high, about 10^8 s^{-1} ion collisions for a $1 \mu\text{m}^2$ grain at $t = 10^7$ s. The associated heating rate $5 - 10 \text{ erg s}^{-1}$ keeps the grain above 1000K but does not evaporate it. The collision energy is roughly equal to that of a well studied natural phenomenon, the solar-wind bombardment of small surface grains on the moon; but the rate of collisions is much smaller on the moon and the lunar grains remain cold.

Profiles of ion implantation have been measured for the lunar soils (Kiko et al. 1978; Zinner et al. 1978). Kiko et al. describe stepwise heating release from individual olivine crystals showing “bimodal release patterns of Ne and Ar atoms, corresponding to a saturated highly radiation damaged 30 nm surface layer and a less damaged zone underneath which is populated by range straggling of solar wind.” Their Figure 5 shows ranges calculated by Lindhard theory for 1 keV amu^{-1} ions of He, Ne and Ar indicating that concentrations 1/10 of maximum are at depths 60 nm for Ar, 45 nm for Ne and 30 nm for He. This depth approximately doubles for speeds of 2 keV amu^{-1} . At the same time the lunar grains are sputtered away slowly; and this will occur in the supernova as well, with O atoms rather than He being the major sputterers.

In the simplest picture, refractory gas atoms in the supernova (C, Si, Ti, Fe, etc.) will be implanted into a skin perhaps 50 - 100 nm thick and that skin will subsequently be sputtered away (primarily by O impacts). The grain core might be thought to remain isotopically unaffected in that picture. However, we point to three aspects of the supernova problem that increase the diffusivity of supernova implanted ions in comparison with the lunar case; namely, mean temperature

above 1000 K and both temperature spikes and radiation damage by intense cosmic-ray acceleration between the forward and reverse shocks. Higher T increases diffusivity in equilibrium crystals. Accelerated particles burst through the entire grain, leaving chemical excitations in their wake and local thermal spikes that may enhance diffusion. We suggest that detailed study of these effects are necessary before concluding that ion implantation cannot alter the grain core. Furthermore, it will be necessary to consider non-thermal events that the grain experiences during its perhaps 10^9 yr residence in the ISM before incorporation into the meteorite. Although arguments that the grain cores will not contain implanted ions must be addressed, it is equally necessary that future work consider imaginatively the total integrated histories of the presolar grains.

6.4. Grain Aggregates

In general, grains condensed farther out in mass coordinate will be moving faster than those condensed more centrally. Therefore grains will not routinely overtake other grains. We note two exceptions to that general expectation. Firstly, turbulent gases will cause grains to collide, perhaps even destructively. Instabilities in the thin dense shell may cause differential grain speeds. We will not address this further, although it may be more important than the second reason. Namely, small grains can be overtaken by larger ones formed interior to them because the small grains decelerate more rapidly than the larger ones. This must certainly occur with or without turbulence.

If the homologous expansion at the time of arrival of a reverse shock at radius r is given by $v = H(t)r$ for matter within the shock. As shown in Figure 5, grains existing at $r - \Delta r$ at the same time t will, after the shock reaches $r - \Delta r$, initially drift more slowly through the shocked and decelerated gas by an amount

$$\Delta v_g = -H(t)\Delta r \quad (8)$$

Each grain loses drift speed at a rate given approximately by

$$m \frac{dv_g}{dt} = -K a^2 \quad (9)$$

where a is the radius of the grain. This formula assumes that the momentum loss by a fast grain is proportional to the rate at which its area impacts slower gas atoms. Since $m = \rho a^3$, the simplest expectation becomes $dv_g/dt = -K'/a$; for example, a 0.1 micron grain loses drift speed ten times faster than a 1 micron grain. This is a general expectation.

The result is that larger grains continuously overtake smaller ones. They collide at relative speeds that are much less than their actual drift speeds with respect to the gas. We anticipate that hot grains can stick together at these low relative speeds, thereby growing grain aggregates, although we can present no evidence to support this expectation. Visual inspection of many SiC X grains (such as in Figure 1) show features that look like grain assemblages; but this may simply be a property of the SiC crystals themselves. Isotopic variations, if detected, could provide such evidence. It is our hope that the new nanoSIMS technology (for an overview of nanonSIMS, see Stadermann et al. 1999) will enable the study of isotopic evidence from distinct subregions of a

grain. For SiC, examination of Figure 10 shows the sense of this to be that large ^{28}Si -rich grains overtake smaller grains having higher $^{29,30}\text{Si}$ fractions. In fact, this aggregation idea predicts such subgrains much richer in $^{29,30}\text{Si}$. This presents another way for grain aggregates to acquire their $^{29,30}\text{Si}$ content, despite many questions that must be addressed. This rate of $^{29,30}\text{Si}$ enrichment may even be more effective than the direct implantation from the $^{29,30}\text{Si}$ -rich gas. And either mechanism suggests a possible reason for SiC X grains to typically have about half the solar fractions of the heavy Si isotopes.

7. Discussion of Other Isotopes

Although SiC grains are built from Si and C atoms, isotopic compositions of trace elements have been significant in defining the X-grain class and in attributing them to supernovae (Amari et al. 2001). We here comment on four elements, N, Al, Mo, and Fe, for which good data exist and for which the consequences of reverse shocks may be significant. These illustrate both successes and puzzles of our model, as well as uses of Tables 2 and 3, which may be of interest to a wide range of other elements, eventually.

7.1. Nitrogen

Table 3 shows that all large SiC condensates, if initially condensed from the range $2.7 < m < 3.3$ as we have argued, will implant $^{14}\text{N}/^{15}\text{N}$ isotopic ratios between 7 and 9, much smaller than the terrestrial value, 272. In other words, the implanted atoms will be ^{15}N -rich. The ^{15}N richness of the SiC X grains has been taken as an indication of their supernova origin (strongly contrasted with N in mainstream SiC, for example), and even as a diagnostic for X-grain classification (Amari et al. 2001). But the measured X-grain ratios are not this ^{15}N -rich, lying mostly in the range 20 to 100, with 50 a typical value. The problem within X grains, therefore, is not "why are they ^{15}N -rich", but "where do they get so much ^{14}N ". Although ion implantation is an attractive possibility, Table 3 shows that it is not an adequate source of ^{14}N . Our model therefore succeeds in explaining the ^{15}N richness, but we must seek other physical grounds for the high ^{14}N content. Although it goes far beyond the aims of this work, we point out that the grains still move fast as they leave the contact discontinuity in the absence of an early shock from the presupernova wind. Implantation of ^{14}N -rich atoms will continue as the grain slows down and even afterward, when interstellar shock waves drive suprathermal ^{14}N ions into all interstellar grains. We thus suggest that the ^{14}N in the X grains may arise primarily from ISM collisions. But it must also be considered that small ^{14}N -rich Si_3N_4 grains, or even graphite, may have formed in the ^{14}N -rich helium shell and may have been overtaken and gathered by the faster moving (after deceleration) large SiC X grains from the core. In such an interpretation, the large ^{15}N -rich SuNoCon may overtake and aggregate ^{14}N -rich smaller grains that initially condensed at greater radii. The new degree of freedom occurs if the smaller grains that condensed further out condensed N more efficiently, or held onto it more efficiently in

the face of sputtering, than the large ^{15}N -rich SuNoCons from the basic SiC condensation zone. The N may condense as refractory AlN or Si_3N_4 within these smaller, overtaken grains, for example. In either case, the natural explanation of N isotopes in X grains may be within reach.

7.2. Aluminum

The case of ^{26}Al has been especially vexing for X-grain interpretation. One of the defining properties identifying the X grain as a SuNoCon is the large isotopic ratio $^{26}\text{Al}/^{27}\text{Al}$ that most contained at the time they solidified, or as we would extend to in the context of this paper, at the time they ceased to take on further supernova atoms. This ratio is measured by the large excess of ^{26}Mg in these grains. It is usually the dominant Mg isotope, because SiC condenses Al much more favorably than it does Mg. Thus the nearly monoisotopic ^{26}Mg was actually ^{26}Al , and the measured initial $^{26}\text{Al}/^{27}\text{Al}$ ratios find almost half are greater than 0.1. The observed $^{26}\text{Al}/^{27}\text{Al}$ initial ratios within the X grain are rather large for the SiC growth zones tabulated in Table 3, which are 3.5×10^{-3} for the implanted-ion ratio. Although that ratio is suitable for some measured X grains, others carry values up to 0.6. Furthermore, Al is able to condense at high T within SiC, so that it is not necessary that the implanted ions dominate the Al budget. An X grain may carry 10^9 - 10^{10} Al atoms, comparable to the number implanted in Table 3 for a shock at 10^9s . This Al-isotope problem has been severe enough to have caused Clayton et al. (1997b) to show that the explosive He cap on a certain class of Type Ia supernova is superior in naturally yielding such a large $^{26}\text{Al}/^{27}\text{Al}$ ratio. The large $^{27}\text{Al}/^{27}\text{Al}$ ratios in the Type II supernova model occur in the He zone and in the H-burning shell, far above the condensation zone for SiC. We call to mind the N discussion above to note that AlN condensed in that material will be both ^{26}Al -rich and ^{14}N -rich, suggesting that assimilation of these small AlN grains by the faster moving large SiC grain could, in principle, provide both the needed ^{14}N and ^{26}Al . But this speculation too exceeds what we have shown.

7.3. Molybdenum

The case of molybdenum came to the fore as the result of new ion-probe techniques called CHARISMA (Pellin, Calaway, Davis, Lewis, Amari, & Clayton 2000). Four of seven X grains studied in this way contained an initially surprising excesses of ^{95}Mo and ^{97}Mo . Since Meyer, Clayton, & The (2000) had shown that this unexpected isotopic richness of odd-A Mo isotopes was the result of rapid neutron captures in the element Zr, an event that called for local bursts of neutrons in the burning shells at the time of passage of the forward shock, it became puzzling why so many SiC X grains would have condensed in such burning shells. The reverse shocks add new dimension to this (Clayton et al. 2002). One can suppose that the moving SiC grains implant Mo atoms, and that therefore the frequency of occurrence of these odd-A excesses can be high. First consider that the Mo atoms may have been implanted. Table 3 shows that although ^{95}Mo but not

^{97}Mo are somewhat enriched (measured relative to ^{96}Mo) in the implanted column, so too is ^{98}Mo but not ^{100}Mo . X grains measured by Pellin et al. (2000) have suggestively similar features, but also differences. Grain 209-1 has the largest excesses relative to ^{96}Mo , namely 83% for ^{95}Mo and 70% for ^{97}Mo , but also carries a 30% excess of ^{98}Mo and no excess of ^{100}Mo . Detailed analysis of this example also takes us beyond the goals of this paper. What we now point out is that a significant fraction of the Mo isotopes may also have been condensed rather than implanted. Figure 14 shows isotopic abundance ratios to ^{96}Mo as a function of mass zone in the SiC condensation zone. The region between $2.7 < m < 3.0$ is unique in having large overabundances of only ^{95}Mo

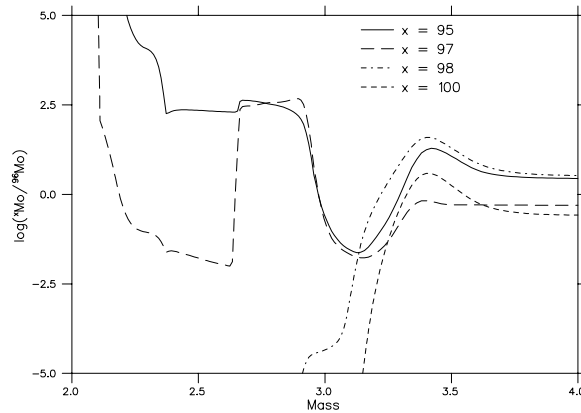


Fig. 14.— *Mass fractions of selected Mo isotopes normalized to the mass fraction of ^{96}Mo , plotted versus mass coordinate. Only the region between $2.6 < m < 3.0$ has a marked overabundance of ^{95}Mo and ^{97}Mo .*

and ^{97}Mo . That this is in the favored condensation zone suggests that condensation of Mo along with the SiC was also important to the Mo budget in the X grains. There does also exist another region of $^{95,97}\text{Mo}$ excess in the He burning shell (at $m = 7$ in the model used here); but ^{98}Mo is also abundant in that shell. Our conclusions from this limited discussion would then be that the Mo atoms may all have been implanted, but that for grains rich in $^{95,97}\text{Mo}$ but not in ^{98}Mo (if such exist) the condensation component for Mo is primarily responsible.

7.4. Iron

The excesses of ^{58}Fe in SiC X grains provided Clayton et al. (2002) with evidence in support of the importance of reverse shocks and implantation of Fe atoms after that shock. Table 3 corroborates this numerically. The number of ^{58}Fe atoms encountered after the shock at 10^9s is from 1.4 to 1.8 times greater than the number of ^{56}Fe atoms encountered, for all condensation zones listed. The total number of Fe atoms in an X grain may be $10^8 - 10^9$, comparable to the number of ^{58}Fe atoms encountered in Table 3. This means that the implanted component can account only for ^{58}Fe , and that most of the remaining Fe atoms must instead have condensed within the SiC. A large

plateau of ^{54}Fe excess lies just barely inside the SiC condensation zone $2.7 < m < 3.2$, and even at $m = 2.7$ it remains the most overabundant Fe isotope. It follows that ^{54}Fe overabundance in X grains comes about as a result of condensation near the inner boundary of the SiC condensation zone or by virtue of significant instability and mixing between $m = 2.5$ and $m = 3.0$.

Tables 2 and 3 may also be used to estimate the numbers of Fe atoms that are available for condensation as might occur if the reverse shock arrived early enough that the growing SiC is stopped before leaving the core. For a reverse shock at 3 yr, as could occur from a large presupernova mass loss, the ion columns are 100 times greater than those listed in Table 2, in which case a SiC that began condensing at $m = 2.7$ would move forward to perhaps $m = 3.3$, by which time the encountered Si column would equal the mass of the grain. The composition of Fe encountered during that scenario would then approximately equal the difference between the column above $m = 2.7$ and the column above $m = 3.3$. That difference in Table 2 is clearly also ^{58}Fe -rich. By this we intend only to illustrate the possible uses of Tables 2 and 3, which appear much more completely in the electronic tables.

8. Summary and Conclusion

Our effort to understand why and how X-type SiC presolar grains condensed within supernova interiors prior to any mixing with circumstellar matter has produced several new discoveries and several hypotheses. They are:

1. Only where $n(\text{Si}) > n(\text{C})$ can SiC condense because graphite normally condenses prior to SiC and exhausts the C. In the absence of specific kinetic condensation model for SiC, we take the thermal equilibrium guidelines to suggest that $n(\text{Si}) > 10 n(\text{C})$ is required.

2. In the new $25M_{\odot}$ model by WHW, SiC condenses between $2.7 < m < 3.2$ because of conclusion 1.

3. Prior to condensation, a reverse shock is returned to the core by the deceleration of the outward moving shock while it propagates through the H envelope. That deceleration happens because of the radial increase of the product ρr^3 within the H envelope, and causes the pileup of hot gas that sends the inward pressure wave. After about 10^6 s this reverse shock creates a high density shell between $2.7 < m < 3.6$, where the density is 10^2 greater than in neighboring mass zones. This high density is maintained by momentum flux into that region, which has higher pressure than the surroundings.

4. The mass zones $n(\text{Si}) > 10 n(\text{C})$ lie within the inner part of that high-density shell, between $2.7 < m < 3.2$, which is therefore where SiC SuNoCons condense. At larger m graphite condenses instead of SiC.

5. The excess O does not lock up the Si and C atoms owing to the radioactive disruption of SiO and CO, allowing carbonaceous condensation in oxidizing gas (Clayton et al. 1999).

6. The ^{28}Si -richness of X grains of SiC is explained by the isotopic constitution of the SiC condensing shell $2.7 < m < 3.2$. We also suggest that the local nucleosynthesis in this shell in the presolar supernovae that parented the X grains produced silicon that is isotopically lighter than in

the WHW calculation for solar metallicity by a factor two owing to the secondary-nucleosynthesis properties of the heavy isotopes of Si (Timmes & Clayton 1996). These factors conspire to explain the absence of supernova SiC SuNoCons having isotopically heavy Si.

7. Between 10^7 s and 10^9 s a second reverse shock moves inward through the mass of the core. It is launched by the collision of the outward shock with the presupernova wind (Chevalier & Fransson 1994). In the WHW $25M_{\odot}$ model the circumstellar wind is $12M_{\odot}$ at the time of the explosion. This shock decelerates the gas to about 60% of its preshock velocity (Truelove & McKee 1999).

8. Following the preceeding reverse shock, the already condensed SuNoCons move forward rapidly through the decelerated gas. Their radial speed is equal to their preshock speed. Thus the grains move forward through the overlying gas at a relative speed that is initially near 40% of their preshock speed, roughly $500\text{--}600 \text{ km s}^{-1}$ for matter near $m = 3$ in the $25M_{\odot}$ WHW model.

9. The forward moving grains implant struck atoms to depths near $0.05 \mu\text{m}$, causing change in the isotopic composition of the SuNoCon (Clayton et al. 2002). The 500 km s^{-1} collisions also cause sputtering of the grains, primarily by O atoms.

10. Owing to the overlying column, the SuNoCons decelerate with respect to the gas until they move with the gas. Because the SuNoCons remain cool, about 1000K , condensation of hot atoms (10^6K) from the local gas continues. This causes mixing of the isotopic composition of the condensate. It is a new physical environment for condensation.

11. As grains decelerate, large grains overtake smaller hot grains at low relative speeds, perhaps allowing them to coalesce. This also causes isotopic mixing of the evolving SuNoCon. Both 10 and 11 may explain when the heavy Si isotopes and the ^{58}Fe isotope are added to the SuNoCon (Clayton et al. 2002). This may also explain why these grains often look like the assemblages of smaller grains (Figure 1).

12. We calculate and tabulate the numbers of atoms in the column overlying a SuNoCon that is already condensed at mass coordinate r_0 at time t_0 when the reverse shock arrives. Several cosmochemical applications are illustrated by the composition of this column.

13. We calculate the numbers of atoms in the overlying column of 12 also taking into account the continuing expansion of the supernova while the grain propagates through that column.

14. Between 10^9 s and 10^{11} s, a third reverse shock propagates into the supernova mass owing to collision of the outward shock with the external ISM. Differential motion of grains and gas occurs again, allowing further sputtering and ion implantation. The altered SuNoCon emerges from the contact discontinuity into the ISM.

Each of these topics raises many additional questions that have not yet been answered. We discussed many of these: the need for 3-D hydrodynamic simulations; the need to study simultaneous turbulent and molecular diffusion; whether the isotopically anomalous skin of a SuNoCon can be homogenized within its bulk; detailed motion of grains relative to gas; whether hot grains coalesce in low speed collisions; the origin of TiC subgrains within the SiC; the actual kinetic description of SiC condensation. These many uncertainties and new questions notwithstanding, we have presented a physical road map to the existence and properties of presolar SiC grains from supernovae, and how they contain information about the young supernova remnant.

Research by ED and DDC is supported by the National Aeronautics and Space Administration under Grant NAG5-11871 issued through the Office of Space Science

AH is supported in part by the Department of Energy under grant B341495 to the Center for Astrophysical Thermonuclear Flashes at the University of Chicago and acknowledges support by a Fermi Fellowship of the Enrico Fermi Institute at The University of Chicago.

REFERENCES

- Amari, S., Hoppe, P., Zinner, E., & Lewis, R. S. 1992, ApJ, 394, L43
- Amari, S., Nittler, L. R., Zinner, E., Lodders, K., & Lewis, R. S. 2001, ApJ, 559, 463
- Bernatowicz, T. J., Cowsik, R., Gibbons, P. C., Lodders, K., Fegley, B. J., Amari, S., & Lewis, R. S. 1996, ApJ, 472, 760
- Bernatowicz, T. J. & Zinner, E., eds. 1997, Astrophysical implications of the laboratory study of presolar materials
- Chevalier, R. A. & Fransson, C. 1994, ApJ, 420, 268
- Clayton, D. 1999, in Astronomy with Radioactivities, eds. R Diehl and D. Hartmann (Max Planck Institute, Munich) publication MPE 274, 175
- Clayton, D. D., Amari, S., & Zinner, E. 1997a, Ap&SS, 251, 355
- Clayton, D. D., Arnett, D., Kane, J., & Meyer, B. S. 1997b, ApJ, 486, 824
- Clayton, D. D., Deneault, E. A.-N., & Meyer, B. S. 2001, ApJ, 562, 480
- Clayton, D. D., Liu, W., & Dalgarno, A. 1999, Science, 283, 1290
- Clayton, D. D., Meyer, B. S., The, L., & El Eid, M. F. 2002, ApJ, 578, L83

Table 1. $(^i\text{Si}/^{28}\text{Si})/(^i\text{Si}/^{28}\text{Si})_{\odot}$ From a Half-Solar Metallicity $25M_{\odot}$ Star

Δm	$^{29}\text{Si}/^{28}\text{Si}$	$^{30}\text{Si}/^{28}\text{Si}$
2.7 - $3.0M_{\odot}$	0.18	0.51
2.7 - $3.2M_{\odot}$	0.29	0.76
2.7 - $3.6M_{\odot}$	0.46	0.95

Table 2. Number of Atoms in a Static Column at 10^9 s for Selected Isotopes ^a

Isotope	Grain Condenses At			
	2.7M _⊙	2.9M _⊙	3.1M _⊙	3.3M _⊙
¹⁴ N	1.366×10^{10}	1.366×10^{10}	1.366×10^{10}	1.366×10^{10}
¹⁵ N	1.562×10^8	1.503×10^8	1.436×10^8	1.374×10^8
²⁶ Al	6.925×10^7	6.919×10^7	6.842×10^7	5.860×10^7
²⁷ Al	2.269×10^{10}	2.235×10^{10}	2.105×10^{10}	1.898×10^{10}
²⁸ Si	1.197×10^{11}	6.879×10^{10}	3.630×10^{10}	2.042×10^{10}
²⁹ Si	9.646×10^9	9.040×10^9	7.612×10^9	5.772×10^9
³⁰ Si	9.894×10^9	8.714×10^9	6.197×10^9	3.628×10^9
⁵⁴ Fe	4.495×10^7	4.305×10^7	4.258×10^7	4.253×10^7
⁵⁶ Fe	8.163×10^8	7.953×10^8	7.866×10^8	7.845×10^8
⁵⁷ Fe	7.347×10^7	7.329×10^7	7.269×10^7	7.145×10^7
⁵⁸ Fe	3.035×10^8	3.022×10^8	2.951×10^8	2.808×10^8
⁹² Mo	3.647×10^3	1.439×10^3	2.887×10^2	2.878×10^2
⁹⁴ Mo	2.579×10^3	2.539×10^3	5.334×10^2	2.431×10^2
⁹⁵ Mo	2.910×10^4	2.909×10^4	2.905×10^4	2.885×10^4
⁹⁶ Mo	1.378×10^4	1.378×10^4	1.315×10^4	1.076×10^4
⁹⁷ Mo	6.540×10^3	6.525×10^3	6.496×10^3	6.433×10^3
⁹⁸ Mo	3.524×10^4	3.524×10^4	3.524×10^4	3.359×10^4
¹⁰⁰ Mo	2.937×10^3	2.937×10^3	2.937×10^3	2.896×10^3

^aThese quantities signify the upper limit on the number of possible interactions of the isotope with the grain. Number of atoms in $1 \mu\text{m}^2$ static column following a reverse shock at 10^9 s. Numbers scale as $(10^9\text{s}/t_0)^2$

Table 3. Number of Atoms in a Moving Column ^afor a Shock Time 10^9 s for Selected Isotopes ^b

Isotope	Grain Condenses At			
	2.7M _⊙	2.9M _⊙	3.1M _⊙	3.3M _⊙
¹⁴ N	6.105×10^8	6.109×10^8	6.111×10^8	6.113×10^8
¹⁵ N	8.584×10^7	8.023×10^7	7.370×10^7	6.763×10^7
²⁶ Al	5.336×10^7	5.347×10^7	5.280×10^7	4.308×10^7
²⁷ Al	1.577×10^{10}	1.549×10^{10}	1.422×10^{10}	1.217×10^{10}
²⁸ Si	1.128×10^{11}	6.226×10^{10}	2.986×10^{10}	1.403×10^{10}
²⁹ Si	8.029×10^9	7.449×10^9	6.035×10^9	4.204×10^9
³⁰ Si	8.855×10^9	7.703×10^9	5.199×10^9	2.639×10^9
⁵⁴ Fe	4.829×10^6	2.939×10^6	2.469×10^6	2.426×10^6
⁵⁶ Fe	1.091×10^8	8.842×10^7	7.989×10^7	7.789×10^7
⁵⁷ Fe	2.293×10^7	2.281×10^7	2.224×10^7	2.104×10^7
⁵⁸ Fe	1.540×10^8	1.531×10^8	1.463×10^8	1.322×10^8
⁹² Mo	3.365×10^3	1.165×10^3	1.628×10^1	1.534×10^1
⁹⁴ Mo	2.353×10^3	2.321×10^3	3.183×10^2	2.818×10^1
⁹⁵ Mo	1.531×10^4	1.534×10^4	1.534×10^4	1.516×10^4
⁹⁶ Mo	7.832×10^3	7.855×10^3	7.240×10^3	4.867×10^3
⁹⁷ Mo	2.614×10^3	2.606×10^3	2.581×10^3	2.521×10^3
⁹⁸ Mo	2.181×10^4	2.188×10^4	2.192×10^4	2.031×10^4
¹⁰⁰ Mo	1.658×10^3	1.663×10^3	1.665×10^3	1.627×10^3

^aColumn limits are from condensation m to the contact discontinuity.

^bNumber of atoms per $1\mu\text{m}^2$, Distance parameter, $t_0\Delta V = 5 \times 10^{16}\text{cm}$

Note. — The full, machine readable version of this table is available in the paper’s electronic supplement.

- Clayton, D. D., Meyer, B. S., & The, L.-S. 2000, in Lunar and Planetary Institute Conference Abstracts, Vol. 31, 1032–+
- Fransson, C., Chevalier, R. A., Filippenko, A. V., Leibundgut, B., Barth, A. J., Fesen, R. A., Kirshner, R. P., Leonard, D. C., Li, W., Lundqvist, P., Sollerman, J., & Van Dyk, S. D. 2002, *ApJ*, 572, 350
- Herant, M. & Woosley, S. E. 1994, *ApJ*, 425, 814
- Kifonidis, K., Plewa, T., Janka, H.-T., & Müller, E. 2000, *ApJ*, 531, L123
- Kiko, J., Kirsten, T., & Ries, D. 1978, in Lunar and Planetary Science Conference, Vol. 9, 1655–1665
- Meyer, B. S., Clayton, D. D., & The, L.-S. 2000, *ApJ*, 540, L49
- Pellin, M. J., Calaway, W. F., Davis, A. M., Lewis, R. S., Amari, S., & Clayton, R. N. 2000, in Lunar and Planetary Science Conference, Vol. 31, 1917
- Rauscher, T., Heger, A., Hoffman, R. D., & Woosley, S. E. 2002, *ApJ*, 576, 323
- Sharp, C. M. & Wasserburg, G. J. 1995, *Geochim. Cosmochim. Acta*, 59, 1633
- Stadermann, F. J., Walker, R. M., & Zinner, E. 1999, *Meteoritics & Planetary Science*, vol. 34, Supplement, p.A111, 34, 111
- Timmes, F. X. & Clayton, D. D. 1996, *ApJ*, 472, 723
- Travaglio, C., Gallino, R., Amari, S., Zinner, E., Woosley, S., & Lewis, R. S. 1999, *ApJ*, 510, 325
- Truelove, J. K. & McKee, C. F. 1999, *ApJS*, 120, 299
- Woosley, S. E., Heger, A., & Weaver, T. A. 2002, *RMP*, 74, In Press
- Zinner, E., Dust, S., Chaumont, J., & Dran, J. C. 1978, in Lunar and Planetary Science Conference, Vol. 9, 1667–1687